

# Understanding Open-Set Recognition by Jacobian Norm of Representation

Jaewoo Park, Hojin Park, Eunju Jeong, Andrew Beng Jin Teoh, *Senior Member, IEEE*,

**Abstract**—In contrast to conventional closed-set recognition, open-set recognition (OSR) assumes the presence of an unknown class, which is not seen to a model during training. One predominant approach in OSR is metric learning, where a model is trained to separate the inter-class representations of known class data. Numerous works in OSR reported that, even though the models are trained only with the known class data, the models become aware of the unknown, and learn to separate the unknown class representations from the known class representations. This paper analyzes this emergent phenomenon by observing the Jacobian norm of representation. We theoretically show that minimizing the intra-class distances within the known set reduces the Jacobian norm of known class representations while maximizing the inter-class distances within the known set increases the Jacobian norm of the unknown class. The closed-set metric learning thus separates the unknown from the known by forcing their Jacobian norm values to differ. We empirically validate our theoretical framework with ample pieces of evidence using standard OSR datasets. Moreover, under our theoretical framework, we explain how the standard deep learning techniques can be helpful for OSR and use the framework as a guiding principle to develop an effective OSR model.

**Index Terms**—Open-Set Recognition, Representation Learning, Out-of-Distribution Detection.

## I. INTRODUCTION

IN recent years, deep neural network (DNN) based models have demonstrated remarkable success in *closed-set recognition*, where the train and test sets share the same categorical classes to classify. In practical environments, however, a deployed model can encounter instances of class categories *unknown* (or unseen) during its training. Detecting these unknown class instances is crucial in safety-critical applications such as autonomous driving and cybersecurity. A solution to this is *open-set recognition* (OSR), where a classifier trained over  $K$  known classes can classify them and reject unknown class instances in the test stage.

A predominant approach in DNN-based OSR and out-of-distribution detection (OoD) is to train a discriminative model over known classes with a metric-learning loss and derive a score (or decision) function that captures the difference

This work was supported by the National Research Foundation of Korea (NRF) grant funded by the Korea government (MSIP) (NO. NRF-2022R1A2C1010710). (Hojin Park and Eunju Jeong have contributed equally to this work.) (*Corresponding Author: Andrew Beng Jin Teoh*)

Jaewoo Park, Hojin Park, and Andrew Beng Jin Teoh are with the School of Electrical and Electronic Engineering, College of Engineering, Yonsei University, Seoul 120749, South Korea. (e-mail:julypraise@yonsei.ac.kr, 2014142100@yonsei.ac.kr, bjteoh@yonsei.ac.kr)

Eunju Jeong is with Woowa Brothers Corp., Seoul 05544, South Korea. (e-mail:eunju.jeong@woowahan.com)

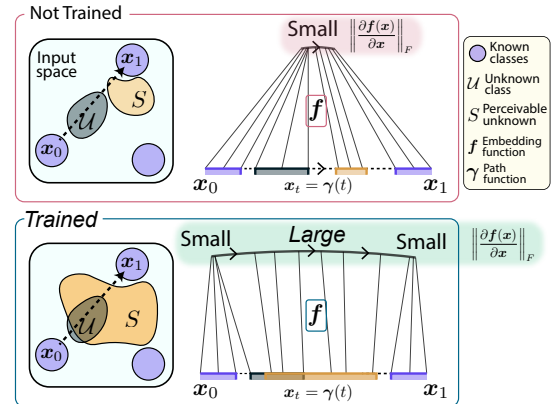


Fig. 1. During the closed-set metric learning over the known classes  $C_k$  (e.g., CIFAR10), the model minimizes the intra-class distances and maximizes inter-class distances in the representation space. Accordingly, the Jacobian norm  $\|\frac{\partial f}{\partial x}\|_F$  of representation embedding  $f$  is minimized over the known set  $\mathcal{K} = \bigcup_k C_k$ , while it is increased over the complement of known set, that is, over the open set  $\mathcal{O}$ . In particular, the inter-class distance maximization enlarges the region  $S := \{x \in \mathcal{O} : \|\frac{\partial f}{\partial x}\|_F > 0\}$  where the Jacobian norm of representation is high. Thus, the inter-class distance maximization increases the overlap  $S \cap U$  between the high Jacobian norm region  $S$  and a given unknown class data  $U$  (e.g., SVHN). As the Jacobian norm is relatively small over the known, the unknown class is separated from the unknown in the representation space by the Jacobian norm difference.

between the representations of known classes and those of the unknown class. For the score function to work correctly, the representations of the unknown class should be separated from the known class representations in the first place. [1] along with subsequent works [2]–[4] observed that training *over known classes alone* with metric-learning losses indeed produces a separation between the known and unknown in the representation space, even though the models never utilize any unknown class sample during training. In other words, the class separation within known classes in the representation space is naturally extended to the separation between the known and unknown.

However, the underlying mechanism of this phenomenon has rarely been explored in the context of representation learning. This work aims to analyze this phenomenon, namely, how the closed-set metric learning entails OSR from a different perspective and provides a fresh perspective based on the **Jacobian norm of the representation**. The Jacobian norm  $\|\frac{\partial f(x)}{\partial x}\|_F$ , which is the Frobenius norm of the Jacobian matrix, quantifies the rate of change in the representation vector  $f(x)$  with respect to its data input  $x$ . We find that the closed-set metric learning reduces this change rate over known classes while increasing the change rate over the un-

known class. In other words, by metric learning, the Jacobian norm of representation is reduced over known classes while increased over the unknown class. Then, this **Jacobian norm difference** between the known and unknown contributes to their separation (as illustrated in Fig. 1).

We theoretically verify this principle by disentangling the roles of intra-class distance minimization and inter-class maximization in closed-set metric learning. In particular, we find that intra-class distance minimization is responsible for reducing the Jacobian norm over the known classes near zero. On the other hand, the inter-class distance maximization contributes to increasing the volume of the high Jacobian norm region within the open set. Then, as the volume of the high Jacobian norm region increases, a given unknown class is more likely to fall into this region. Thus, for sufficiently strong inter-class distance maximization, an unknown class sample involves a relatively high Jacobian norm compared to the known class samples. This Jacobian norm difference separates the known and unknown classes in the representation space.

We empirically validate our theoretical analysis in diverse aspects by analyzing the standard metric-learning models over the multiple OSR datasets. In addition, we find strong correlations between three metrics: the Jacobian norm difference, the degree of separation between known and unknown classes, and the degree of separation between different known classes. All these metrics are computed over the representations. Our empirical evidence indicates that the Jacobian norm difference is one of the explanatory factors that disclose why closed-set metric learning entails OSR.

Our theoretical analysis suggests two principles: Firstly, strong inter-class distance maximization is a crucial factor for adequate unknown class representation segregation and, hence, successful OSR. Second, one characteristic that separates the unknown from the known is their difference in the Jacobian norm of representations. Utilizing these analyses as a guiding principle, we develop a method to improve OSR performance effectively. Mainly, we define the unknown class detection score by the model loss function as it captures the increasing/decreasing trend of the Jacobian norm, which is a source of the separation.

Then, we adopt a modified version of one-vs-rest loss, termed marginal one-vs-rest (m-OvR) loss. The m-OvR induces stronger inter-class maximization, better separating the known and unknown class representations. The margin of m-OvR, on the other hand, prevents the collapse of inter-class prototypes that serve as known class proxies in the representation space. Hence, the margin improves the alignment between the data representations and the prototypes, improving the effectiveness of the loss-based unknown class detector. In addition, we utilize weight decay, auxiliary self-supervision, and data augmentation to improve the OSR performance further. These techniques are justified in light of our proposed theory based on the Jacobian norm of representations.

The contributions of our works are summarized as follows:

- 1) We theoretically show that the closed-set metric learning separates the representations of unknown class from those of the known classes by making their Jacobian norm different.

- 2) We empirically validate our theory, observing that the Jacobian norm difference between the known and unknown classes is strongly correlated to the discriminative quality of known class representations and the unknown class detection performance.
- 3) Based on our theory as a guiding principle, we develop an effective OSR model. Our theory suggests which model components are more beneficial than others for OSR under the new perspective of Jacobian norm of representation. Particularly:
  - We justify the loss function as an effective unknown class detector since the loss can capture the trend of the Jacobian norm, which is a main factor that separates the known from the unknown.
  - We justify the usage of the OvR loss and the insertion of margin in the class similarity for improving the OSR performance. Termed by the marginal one-vs-rest (m-OvR), it improves inter-class separation. In addition, it resolves the prototype misalignment issue, enhancing the effectiveness of the loss-based unknown class detector for OSR.
  - We include weight decay, auxiliary self-supervision, and data augmentation in our method as they are shown to improve the Jacobian norm difference.

We highlight that our main objective is not to push the state-of-the-art; instead, **our main contribution is a theoretical understanding of the emergent phenomenon that a closed-set model trained by metric learning becomes aware of the unknown**. Other contributions include the empirical verification of our theory and analysis of widely-used deep learning techniques in the new light of our theory. To our knowledge, we are the first to study OSR representation based on its Jacobian norm.

## II. RELATED WORKS

**Theoretical/empirical works on OSR.** Recent theoretical works [5], [6] tackle OSR with theoretical guarantees on the performance but with specific distributional modeling assumptions (e.g. Gaussian mixture). On the other hand, [7], [8] conduct theoretical studies in a more general setting by extending the classical closed-set PAC framework [9] to open-set environments, deriving analytical bounds of the generalization error in the context of OSR. In particular, [7] relates OSR to transfer learning and interprets the unknown class samples as covariate shifts. This enables the substitution of theoretical bounds derived in the transfer learning setting [10] to open-set environments. On the other hand, [11] observes that for a model trained only with known class samples, the magnitudes of representation vectors tend to exhibit relatively larger values over the known class than over the unknown ones. However, the study does not analyze the underlying principle of the observed characteristic.

**OSR methods.** For a general, broad survey on OSR models, the readers are recommended to [4], [12]. Here, we focus on reviewing state-of-the-art OSR models, mainly focusing on discriminative ones.

The basic baseline model [1], [13], [14] trained by softmax cross-entropy loss is known to perform both closed-set classification and unknown class detection reasonably effectively. To enhance its unknown detection mechanism, OpenMax [15] applied probabilistic modification on the softmax activation based on extreme value theory. DOC [16] replaced the softmax cross entropy with the one-vs-rest logistic regression, finding its effectiveness on invalid topic rejection in natural language. RPL [17] proposed to maximize inter-class separation in the form of reciprocal, followed by a variant [18] that utilizes synthetic, adversarially generated unknown class. CPN [19] learns embedding metrics by modeling each known class as a group of multiple prototypes. PROSER [20] leverages latent mixup samples [21], [22] as a generated unknown class and places their representations near the known class representations. [23], on the other hand, proposed a collection of multiple one-vs-rest networks to mitigate the over-confidence and poor generalization issue, and utilizes a collective decision score for effective OSR. Recently, [14] demonstrated that the basic SCE baseline could outperform all other OSR baselines if the SCE model is trained with strong data augmentation and utilizes state-of-the-art optimization techniques.

### III. THEORY: ANALYSIS OF OSR BY JACOBIAN NORM OF REPRESENTATION

#### A. Problem Setup and Notation

During closed-set metric learning, the representation embedding function  $\mathbf{f} : \mathbb{R}^d \rightarrow \mathbb{R}^{d_z}$  of a discriminative model is trained to minimize *intra-class distances*  $\mathcal{D}(\mathbf{f}(\mathbf{x}), \mathbf{w}_y)$  and maximize *inter-class distances*  $\mathcal{D}(\mathbf{f}(\mathbf{x}), \mathbf{f}(\mathbf{x}'))$  for known class samples  $\mathbf{x}$  and  $\mathbf{x}'$  paired with different class labels  $y$  and  $y'$  ( $y \neq y'$ ). The prototype vector  $\mathbf{w}_y \in \mathbb{R}^{d_z}$  is a proxy for the  $y$ -th known class  $C_y$ , and is formulated as a learnable parameter. The known set  $\mathcal{K} = \cup_{k=1}^K C_k$  consists of  $K$  disjoint disconnected known classes  $C_k$ . The train samples  $\mathbf{x}$  and  $\mathbf{x}'$  are sampled from the known set, while the labels  $y$  and  $y'$  from the corresponding label space  $\mathcal{Y}_{\mathcal{K}} = \{1, \dots, K\}$ . The open set  $\mathcal{O} := \mathcal{X} \setminus \mathcal{K}$  is the complement of the known set in the (bounded) global space  $\mathcal{X} = [-1, 1]^d \subseteq \mathbb{R}^d$ . The unknown class  $\mathcal{U}$  we consider is a *proper* subset of the open set  $\mathcal{O}$ . Since our task is not to discriminate within the unknown class, we treat the unknown class as a single class, although it may consist of a diverse type of object.

During training, the model has no access to the unknown class  $\mathcal{U}$ , and is trained only with the  $K$  number of known classes to discriminate them. After training, the OSR model should not only discriminate each class in the known set but also need to discriminate the unknown from the known. Hence, the unknown class should be separated from all known classes in the representations space.

#### B. Theoretical Analysis

To analyze how the closed-set metric learning entails OSR, we first consider the dynamics of the representations  $\mathbf{f}(\mathbf{x}_t)$  over a class interpolating path  $\mathbf{x}_t = \gamma(t)$ . Here, an arbitrary path  $\gamma: [0, 1] \rightarrow \mathcal{X}$  we consider is regular in the sense that it is a smoothly differentiable simple path (over the closed interval

$[0, 1]$ ) that interpolates two different known classes  $C_i$  and  $C_j$  by traversing  $t$  from 0 to 1 with  $\mathbf{x}_0 \in C_i$  and  $\mathbf{x}_1 \in C_j$  (Fig. 1).

1) *Assumptions and Terminologies*: Before delving into the theoretical derivation, we first rigorously state several assumptions we make and terminologies we use. First of all, the known classes  $C_i$  in the input space (e.g., image pixel space) follow the following regularity:

#### Assumption 1.

- (a) *Each known class  $C_k$  is a simple smooth, connected compact manifold with a nonzero volume.*
- (b) *For any linear path  $\gamma : [0, 1] \rightarrow \mathcal{X}$  from  $C_j$  to  $C_k$ , there exist  $t_1$  and  $t_2$  such that  $\gamma([t_1, t_2]) \subseteq \mathcal{O}$  with  $0 < t_1 < t_2 < 1$*

Note that the volume we refer to in Assumption 1a is the Lebesgue measure in the Euclidean space  $\mathbb{R}^d$ . Assumption 1b indicates that the in-between part of the linear interpolation between different known classes is a part of an open set. This assumption is reasonable since interpolating in a very high-dimensional space, such as image pixel space, always induces meaningless inputs in the middle part of the interpolation.

Now, as to the representation embedding function  $\mathbf{f}$ , we restrict our consideration to the family of neural network-based functions whose metric learning follows the following regularity.

#### Assumption 2.

- (a)  *$\mathbf{f}$  is a bounded smooth parametrized neural network (i.e.,  $\mathbf{f} = \mathbf{f}_\theta$  with a parameter  $\theta$ ) with a sufficient complexity.*
- (b) *For any simple smooth path  $\gamma$  from  $C_j$  to  $C_k$ , maximizing the inter-class distances  $\mathcal{D}(\mathbf{f}(\mathbf{x}), \mathbf{f}(\mathbf{x}'))$  with arbitrary  $\mathbf{x} \in C_j$  and  $\mathbf{x}' \in C_k$  does **not decrease**  $\|\partial \mathbf{f} \circ \gamma / \partial t\|_2$ .*
- (c) *For any **linear** simple smooth path  $\gamma$  from  $C_j$  to  $C_k$ , maximizing the inter-class distances  $\mathcal{D}(\mathbf{f}(\mathbf{x}), \mathbf{f}(\mathbf{x}'))$  with arbitrary  $\mathbf{x} \in C_j$  and  $\mathbf{x}' \in C_k$  **strictly increases** the length of the projected path  $\mathbf{f}(\gamma([0, 1]) \cap \mathcal{O})$ .*

Assumption 2a is a standard regularity condition. Assumption 2b means that inter-class distance maximization at least indicates no harmful behavior when observed locally over the open set. The assumption is reasonable based on the empirical evidence given in Fig. 3. Assumption 2c means that the inter-class separation is effective on the linear interpolating path  $\gamma$ . Assumption 2c is visualized in Fig. 1, which indicates that the length of projected (inter-class) path is strictly increased by metric learning.

In the below mathematical derivations, when we say that a quantity  $Q(\mathbf{f})$  increases with respect to a function  $\mathbf{f} : \mathbb{R}^d \rightarrow \mathbb{R}^{d_z}$ , it formally means that there is a sequence  $(\mathbf{f}^{(n)})_{n=0}^N$  of functions  $\mathbf{f}^{(n)} : \mathbb{R}^d \rightarrow \mathbb{R}^{d_z}$  with  $N \geq 1$  such that

$$Q(\mathbf{f}^{(n)}) \leq Q(\mathbf{f}^{(n+1)}) \quad (1)$$

for all  $0 \leq n < N$ . In the case of a strict increment, the inequality is replaced by the strict one. The decrement of  $Q(\mathbf{f})$  is similarly defined.

Depending on the context,  $Q$  may include the vectors  $\mathbf{w}_k \in \mathbb{R}^{d_z}$  (that serve as representation prototypes in our work):  $Q = Q(\mathbf{f}, \{\mathbf{w}_k\}_{k=1}^K)$ .

2) *Derivation of the Theory:* We now derive the dynamic characteristics of the representation embedding function  $\mathbf{f}$  in the aspects of metric learning by analyzing it on the interpolating path  $\gamma$  between known classes. During the closed-set supervision, the intra-class distance minimization minimizes the length of the projected path over the known class:

**Proposition 1.** *Minimizing intra-class distances  $\mathcal{D}(\mathbf{f}(\mathbf{x}), \mathbf{w}_k)$  to 0 for all  $\mathbf{x} \in C_k$  minimizes the length of the projected path  $\mathbf{f}(\gamma([0, 1]) \cap C_k)$  for an arbitrary path  $\gamma$  from  $C_k$ .*

*Proof.* Fix  $C_k$ . We prove a stronger result that

$$\frac{\partial \mathbf{f}}{\partial \mathbf{x}} \rightarrow \mathbf{0} \in \mathbb{R}^{d_z \times d} \quad (2)$$

for all  $\mathbf{x} \in C_k$ . In which case,  $\frac{d\mathbf{f}(\gamma(t))}{dt} \rightarrow \mathbf{0}$  for all  $t \in \gamma^{-1}(\gamma([0, 1]) \cap C_k)$  since  $\frac{df_j(\gamma(t))}{dt} = \sum_{i=1}^n \frac{\partial f_j}{\partial x_i}(\gamma(t)) \gamma'_i(t)$  for all  $j$  where  $\mathbf{x} = (x_1, \dots, x_d)$  and  $\mathbf{f} = (f_1, \dots, f_{d_z})$ . Then, this implicates that the length of  $\mathbf{f}(\gamma([0, 1]) \cap C_k)$  converges to 0 (as the pointwise convergence guarantees the  $L_p$  convergence when the functions are bounded).

Let  $\mathbf{f}^{(n)} := \mathbf{f}_{\theta^{(n)}}$  be a sequence that minimizes  $\mathcal{D}(\mathbf{f}^{(n)}(\mathbf{x}), \mathbf{w}_k)$  to 0 as  $n \rightarrow N$ . Let  $\mathbf{x} \in C_k$ . Since the quantity at hand is a partial derivative, without loss of generality, assume  $\mathbf{f}(\mathbf{x}) = f(x)$  and  $\mathbf{x} = x$  are scalar-valued (and also for  $\mathbf{w}_k = w_k$ ). Fix  $\epsilon > 0$ . Then for some  $\delta > 0$ , we have

$$\left| \frac{d}{dx} f^{(n)}(x) - \left( \frac{f^{(n)}(x+h) - f^{(n)}(x)}{h} \right) \right| < \epsilon \quad (3)$$

for all  $h \in [-\delta, \delta] \setminus \{0\}$ . Taking  $n \rightarrow N$ , we obtain

$$\left| \lim_{n \rightarrow N} \frac{d}{dx} f^{(n)}(x) - 0 \right| < \epsilon \quad (4)$$

since  $f^{(n)} \rightarrow w_k$ . The arbitrariness of  $\epsilon$  concludes the proof.  $\square$

On the other hand, the inter-class distance maximization is presumed to increase the length of any linear path between the known classes  $C_i$  and  $C_j$  in the representation space by Assumption 2c. In summary, intra-class distance minimization reduces the projected path length, while the inter-class distance maximization increases the projected path length.

Now, the increasing/decreasing trend of the projected path length due to the metric learning is transferred to the Jacobian norm  $\left\| \frac{d\mathbf{f}(\gamma(t))}{dt} \right\|_2$  via the path length equation

$$\text{length}(\mathbf{f} \circ \gamma) = \int_0^1 \left\| \frac{d\mathbf{f}(\gamma(t))}{dt} \right\|_2 dt. \quad (5)$$

Accordingly, we expect that intra-class distance minimization minimizes the Jacobian norm over the known class intersecting path. In contrast, inter-class distance maximization increases the Jacobian norm over the open set intersecting path. This description, however, is constrained to the local paths. The following theorem assures that this phenomenon is extendible from the local path to the global region. In other words, the closed-set metric learning minimizes the Jacobian norm over the known classes and increases the Jacobian norm over the open set  $\mathcal{O}$ .

**Theorem 2.** *Let  $C_i$ ,  $C_j$ , and  $C_k$  be different known classes.*

- (a) *Minimizing intra-class distances  $\mathcal{D}(\mathbf{f}(\mathbf{x}), \mathbf{w}_k)$  for all  $\mathbf{x} \in C_k$  minimizes  $\left\| \frac{\partial \mathbf{f}(\mathbf{x})}{\partial \mathbf{x}} \right\|_F$  over  $C_k$ .*
- (b) *Maximizing inter-class distances  $\mathcal{D}(\mathbf{f}(\mathbf{x}), \mathbf{f}(\mathbf{x}'))$  for all  $\mathbf{x} \in C_i$  and  $\mathbf{x}' \in C_j$  strictly increases  $\int_{\mathcal{O}} \left\| \frac{\partial \mathbf{f}(\mathbf{x})}{\partial \mathbf{x}} \right\|_F d\mathbf{x}$ .*

*Proof.* The intra-class minimization part is proved in the proof of Proposition 1.

For the inter-class maximization part, without loss of generality, redefine  $\mathbf{f}$  such that  $\mathbf{f}(\mathbf{x}) = \mathbf{0}$  for all  $\mathbf{x} \in \mathcal{X} \setminus \mathcal{O}$ , while to be the same as the original  $\mathbf{f}$  over  $\mathcal{O}$ . Now, it suffices to prove the strict increment of  $\int_{\mathcal{X}} \left\| \frac{\partial \mathbf{f}(\mathbf{x})}{\partial \mathbf{x}} \right\|_F d\mathbf{x}$  with respect to this  $\mathbf{f}$ .

Note that Assumption 2b implies that  $\left\| \frac{\partial \mathbf{f} \circ \gamma}{\partial t} \right\|_2$  as a function of  $t$  is non-decreasing with respect to the changing  $f$  for any simple smooth path  $\gamma$ . Hence,  $\left\| \frac{\partial \mathbf{f}}{\partial x_l}(\mathbf{x}) \right\|_2^2$  is non-decreasing for any  $l = 1, \dots, d$ . We use this property freely in the following.

Since  $\text{Vol}(C_i) > 0$  for all known classes  $C_i$ , for any pair of different known classes  $C_i$  and  $C_j$ , we have a  $(d-1)$ -dimensional hyperplane  $P \subseteq \mathcal{X}$  such that

$$\text{Vol}_{d-1}(\rho(C_i) \cap \rho(C_j)) > 0 \quad (6)$$

where  $\text{Vol}_{d-1}$  is the  $(d-1)$ -dimensional volume, and  $\rho(C_i)$  is the projection of  $C_i$  to the hyperplane  $P$ . Since a coordinate change under rotation and translation does not change the volume integral of a function, we assume without loss of generality that

$$\mathbf{e}_k \perp P; \quad (7)$$

that is,  $\mathbf{e}_k$  is perpendicular to  $P$  where  $\mathbf{e}_k$  is the  $k$ -th standard basis element of  $\mathbb{R}^d$ .

Now, observe

$$\int_{\mathcal{X}} \left\| \frac{\partial \mathbf{f}(\mathbf{x})}{\partial \mathbf{x}} \right\|_F^2 d\mathbf{x} = \sum_{l=1}^d \int_{\mathcal{X}} \left\| \frac{\partial \mathbf{f}(\mathbf{x})}{\partial x_l} \right\|_2^2 d\mathbf{x}. \quad (8)$$

Since  $\int_{\mathcal{X}} \left\| \frac{\partial \mathbf{f}(\mathbf{x})}{\partial x_l} \right\|_2^2 d\mathbf{x}$  is non-decreasing for  $l \neq k$ , it suffices to show that  $\int_{\mathcal{X}} \left\| \frac{\partial \mathbf{f}(\mathbf{x})}{\partial x_k} \right\|_2^2 d\mathbf{x}$  is strictly increasing. Let

$$R = \{\hat{\mathbf{x}}_k \in [-1, 1]^{d-1} : \mathbf{x} \in \rho(C_i) \cap \rho(C_j)\}. \quad (9)$$

where  $\hat{\mathbf{x}}_k$  denotes  $\hat{\mathbf{x}}_k := (x_1, \dots, x_{k-1}, x_{k+1}, \dots, x_d)$  that removes the  $k$ -th element of  $\mathbf{x}$ . Note that

$$\begin{aligned} \int_{\mathcal{X}} \left\| \frac{\partial \mathbf{f}(\mathbf{x})}{\partial x_k} \right\|_2^2 d\mathbf{x} &= \int_R \int_{-1}^1 \left\| \frac{\partial \mathbf{f}(\mathbf{x})}{\partial x_k} \right\|_2^2 dx_k d\hat{\mathbf{x}}_k \\ &\quad + \int_{R^c} \int_{-1}^1 \left\| \frac{\partial \mathbf{f}(\mathbf{x})}{\partial x_k} \right\|_2^2 dx_k d\hat{\mathbf{x}}_k \end{aligned} \quad (10)$$

where  $d\hat{\mathbf{x}}_k := dx_1 \cdots dx_{k-1} dx_{k+1} \cdots dx_d$ . Since the second term on the RHS of the above equation is non-decreasing, we consider the first only, whose inner term

$$\int_{-1}^1 \left\| \frac{\partial \mathbf{f}(\mathbf{x})}{\partial x_k} \right\|_2^2 dx_k. \quad (11)$$

is decomposed into

$$\int_{-1}^a + \int_a^b + \int_b^1 \left\| \frac{\partial \mathbf{f}(\mathbf{x})}{\partial x_k} \right\|_2^2 dx_k \quad (12)$$

where the scalars  $a = a(\widehat{\mathbf{x}}_k)$  and  $b = b(\widehat{\mathbf{x}}_k)$  are the infimum and supremum of  $\{x_k : \mathbf{x} \in C_i \cup C_j\}$ , respectively, with  $\widehat{\mathbf{x}}_k \in R$ . The first and third terms non-decrease, thus ignored. To compute the mid term  $\int_a^b \|\frac{\partial \mathbf{f}(\mathbf{x})}{\partial x_k}\|_2^2 dx_k$ , consider a path

$$\gamma(t) = (x_1, \dots, x_{k-1}, a + (b-a)t, x_{k+1}, \dots, x_d) \quad (13)$$

that depends on  $\widehat{\mathbf{x}}_k = (x_1, \dots, x_{k-1}, x_{k+1}, \dots, x_d) \in R$ . Then,  $\gamma$  is a path from  $C_i$  to  $C_j$  or the other way, and

$$\begin{aligned} \int_a^b \left\| \frac{\partial \mathbf{f}(\mathbf{x})}{\partial x_k} \right\|_2^2 dx_k &= (b-a) \int_0^1 \left\| \frac{d\mathbf{f} \circ \gamma(t)}{dt} \right\|_2^2 dt \quad (14) \\ &= (b-a) \ell(\mathbf{f} \circ \gamma) \quad (15) \end{aligned}$$

where  $\ell(\mathbf{f} \circ \gamma) = \int_0^1 \|\frac{d\mathbf{f} \circ \gamma(t)}{dt}\|_2^2 dt$ . In summary,

$$\begin{aligned} \int_{\mathcal{O}} \left\| \frac{\partial \mathbf{f}}{\partial \mathbf{x}}(\mathbf{x}) \right\|_2^2 d\mathbf{x} \\ = A(\mathbf{f}) + \int_R [b(\widehat{\mathbf{x}}_k) - a(\widehat{\mathbf{x}}_k)] \ell(\mathbf{f} \circ \gamma) d\widehat{\mathbf{x}}_k. \quad (16) \end{aligned}$$

Here, the inter-class maximization does not change  $R$ ,  $\widehat{\mathbf{x}}_k$ ,  $\gamma$ ,  $a(\widehat{\mathbf{x}}_k)$ , and  $b(\widehat{\mathbf{x}}_k)$ . On the other hand, the inter-class maximization does not decrease the term  $A(\mathbf{f})$ . Moreover, note that  $\gamma \cap \mathcal{O}$  is not empty and contains an interval by Assumption 1b. Thus, by Assumption 2c, the inter-class maximization strictly increases the term  $\ell(\mathbf{f} \circ \gamma)$ , thereby strictly increasing the global integral of the Jacobian norm over the open set. This finishes the proof.  $\square$

The proof of Theorem 2b indicates that the length of the projected path can be accessed from the global integral of the Jacobian norm. Thereby, we find that the strictly increasing trend of Jacobian norm integral is positively correlated to the strictly increasing trend of the projected inter-class path length.

**Corollary 3.** *Minimizing the intra-class distances minimizes  $\|\frac{\partial \mathbf{f}(\mathbf{x})}{\partial \mathbf{x}}\|_F$  over  $\mathcal{K}$ , while maximizing the inter-class distances strictly increases  $\int_{\mathcal{O}} \|\frac{\partial \mathbf{f}(\mathbf{x})}{\partial \mathbf{x}}\|_F d\mathbf{x}$ .*

Now, the integral  $\int_{\mathcal{O}} \|\frac{\partial \mathbf{f}(\mathbf{x})}{\partial \mathbf{x}}\|_F d\mathbf{x}$  can be decomposed into

$$\int_{\mathcal{O}} \|\frac{\partial \mathbf{f}(\mathbf{x})}{\partial \mathbf{x}}(\mathbf{x})\|_F d\mathbf{x} = \text{Vol}(S) \cdot \mathbb{E}_{\mathbf{x} \sim S} [\|\frac{\partial \mathbf{f}}{\partial \mathbf{x}}(\mathbf{x})\|_F] \quad (17)$$

where  $\mathbf{x} \sim S$  is uniformly sampled, and

$$S := \{\mathbf{x} \in \mathcal{O} : \|\frac{\partial \mathbf{f}(\mathbf{x})}{\partial \mathbf{x}}\|_F > 0\} \quad (18)$$

is the support set of the Jacobian norm over the open set  $\mathcal{O}$ . Based on the decomposition, the inter-class distance maximization increases the volume  $\text{Vol}(S)$  of the set  $S$  and/or the expected Jacobian norm over  $S$ :

**Corollary 4.** *Maximizing inter-class distances between  $C_i$  and  $C_j$  strictly increases*

$$\text{Vol}(S) \text{ and/or } \mathbb{E}_{\mathbf{x} \sim S} [\|\frac{\partial \mathbf{f}}{\partial \mathbf{x}}\|_F]. \quad (19)$$

Thus, for a model trained by metric learning, **the support set  $S$  consists of input samples whose representations have relatively high Jacobian norm**, while the known class input samples (e.g. CIFAR10 samples) involve representations with the small Jacobian norm. This Jacobian norm difference

guarantees the separation between the known class samples and the support set  $S$  samples in the representation space. In this respect, **the region  $S$  of the high Jacobian norm can be regarded as a perceivable unknown class**.

Now, we consider a specific real unknown class  $\mathcal{U}$  (e.g., SVHN) residing inside the open set. Corollary 4 states that inter-class distance maximization increases the volume of the high Jacobian region  $S$ . Hence, it can also increase the overlap  $S \cap \mathcal{U}$  between the high Jacobian norm region  $S$  and the unknown class  $\mathcal{U}$ , which in turn increases the Jacobian norm of unknown class samples in  $\mathcal{U}$ . **Overall, by metric learning, the model increases the expected Jacobian norm difference between the known and unknown**

$$\mathbb{E}_{\mathbf{x} \sim \mathcal{U}} [\|\frac{\partial \mathbf{f}(\mathbf{x})}{\partial \mathbf{x}}\|_F] - \mathbb{E}_{\mathbf{x} \sim \mathcal{K}} [\|\frac{\partial \mathbf{f}(\mathbf{x})}{\partial \mathbf{x}}\|_F]. \quad (20)$$

**The increased Jacobian norm difference then separates the known classes from the unknown class in the representation space.**

Through the paper, the value given in Eq. (20) is referred to by **Jacobian norm difference** (between the known and unknown classes). Our derivations show that the Jacobian norm difference is one factor that explains how the closed-set metric learning induces OSR. Our overall understanding of how the Jacobian norm induces the separation is summarized in Fig. 1.

**Remark (Limitation of the Theory on Jacobian Norm).** We highlight that the Jacobian norm characteristic is **only one of the many explanatory factors** that demystifies how closed-set metric learning derives OSR; our analysis does not fully characterize all connections between closed-set metric learning and OSR. One apparent phenomenon our theory does not explain is that known and unknown representations can be separated in the metric space with having the same Jacobian norm value. Moreover, our theory is limited in characterizing the support set  $S$ . As the support set does not include the whole part of the open set, there would be some unknown class that is not included in the support. In this case, the Jacobian norm difference indicated in Eq. (20) would not be explanatory.

#### IV. EMPIRICAL VERIFICATION OF THE THEORY

In this section, we empirically verify the theory developed in Sec. III in multiple aspects.

##### A. Experiment Setup

We empirically analyze the relationship between the Jacobian norm difference and the unknown class detection to evidence our theoretical analysis. To this end, we train our proposed model as described in Sec. V and VI, and evaluate over OSR datasets described in Sec. VI. We note that the same trend holds for the model trained with a standard softmax cross entropy loss (as shown in Supplementary A). To compute the degree of separation between known and unknown, we use the detection score provided in Sec. V-A and evaluate the area under the receiver-operating-characteristic curve (AUC) metric [24]. The discriminative (cluster) quality of known class representations is measured in Davies-Bouldin Index (DBI)

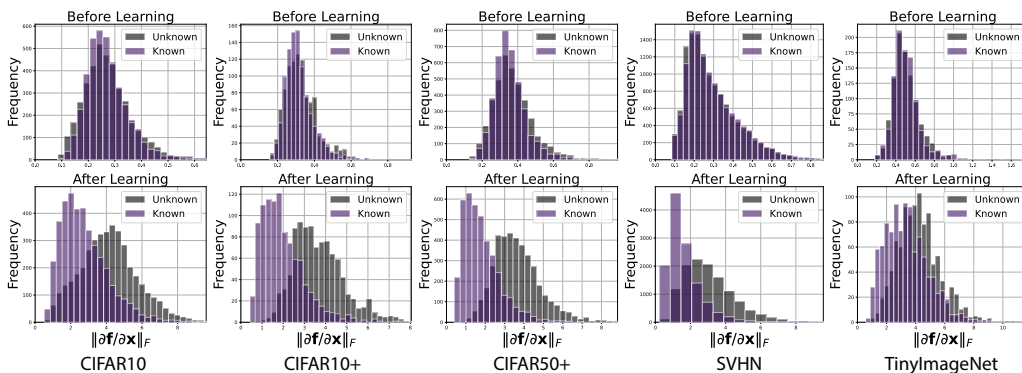


Fig. 2. The distribution of Jacobian norms of representations **before and after training**. Although the model is trained only on the known class data, the model learns to increase the Jacobian norm of unknown class representation, while lowering the Jacobian norm of the known class representation.

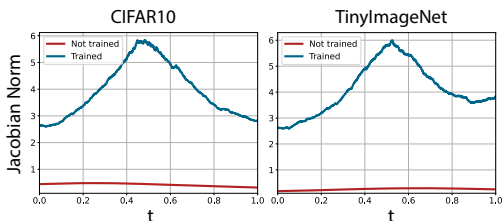


Fig. 3. Given known class samples  $\mathbf{x}_0 \in C_i$  and  $\mathbf{x}_1 \in C_j$  from two different classes  $C_i$  and  $C_j$ , we **linearly interpolate** between  $\mathbf{x}_0$  and  $\mathbf{x}_1$ , obtaining  $\mathbf{x}_t := (1-t)\mathbf{x}_0 + t\mathbf{x}_1$ . Then, we measure the Jacobian norm of the representation  $\mathbf{f}(\mathbf{x}_t)$ . When  $t \approx 0.5$ , the interpolated sample  $\mathbf{x}_t$  passes through the open set, where unknown class samples arise.

[25], which measures the ratio of intra-class distance to inter-class distance. All experiments are conducted with one 12GB GPU RTX 2080-ti. Due to resource limitations, empirical observations are made on standard OSR datasets rather than recently proposed high-resolution OSR datasets [14].

### B. Empirical Observations

**Jacobian norm before and after training.** Fig. 2 demonstrate that the gradient norm separates the representations only after training. Fig. 3 displays the gradient norm over the linearly interpolated data samples  $\mathbf{x}_t$  for  $t \in [0, 1]$  between two different class samples  $\mathbf{x}_0 \in C_i$  and  $\mathbf{x}_1 \in C_j$ . It shows that the interpolated samples inside the open region have a larger gradient norm than those in the known classes. These empirical observations support our theory. In practice, however, inter/intra-class distance optimizations conflict; thus, the overall gradient norm increases for both the known and unknown. Nonetheless, the gradient norm is relatively higher over the unknown class than the known, evidencing our theory. **The dynamics of the Jacobian norm during training.** Fig. 4 shows the dynamics of different quantities during training. The intra/inter-class distance optimization increases the quality of cluster separation measured by DBI. Accordingly, the linear projected path length between different known classes in the representation space increases (Fig. 4b). As a result, the model increases both the Jacobian norm difference (Fig. 4c) and the degree of separation between known and unknown classes (Fig. 4d) as claimed by the theory.

Although the global trend has a simple correspondence between these metrics, a more careful look at the graphs of Fig. 4 shows that the metrics involve different phases during training. Specifically, the intra/inter ratio is stable at the early stage of training. On the other hand, the inter-class distance is still increasing even at a later stage. The Jacobian norm difference rises more gradually, and the rate of increase becomes large at the last stage. The separation between the known and unknown also increases largely at the early stage but continues to improve even later in training. These observations show that the known and unknown class representations are separated as the model makes their Jacobian norm different. Still, the Jacobian norm is not the only factor contributing to their separation.

**The correlation between Jacobian norm and discriminative metrics.** For each dataset, we measure the following three metrics during different training iterations: the discriminatory quality of known class representations (DBI), the unknown class detection performance (AUC), and the averaged Jacobian norm difference between known and unknown classes.

Fig. 5(1st row) shows that the degree of separation between the known and unknown strongly correlates to the Jacobian norm difference. This observation evidences our theoretical claim that the closed-set metric learning separates the unknown by increasing their Jacobian norm difference during training. There is, however, nonlinearity between these two metrics, showing that the Jacobian norm difference is not the only factor contributing to the separation of unknown class representation.

Fig. 5(2nd row) shows a similar correlation trend between the intra/inter-class distance ratio (DBI) and the Jacobian norm difference. However, the nonlinearity between them is severe. The plot indicates that the Jacobian norm difference abruptly increases at a later stage of training where the intra/inter ratio is already small and stable.

**The relation between the Jacobian norm difference and the number of discriminative classes.** Theorem 2 states that the inter-class distance maximization between a single pair of inter classes ( $C_i, C_j$ ) can cause to increase in the Jacobian norm difference. Therefore, we hypothesize that a larger number of inter-class pairs would improve the Jacobian norm difference, contributing to better separation between known and unknown

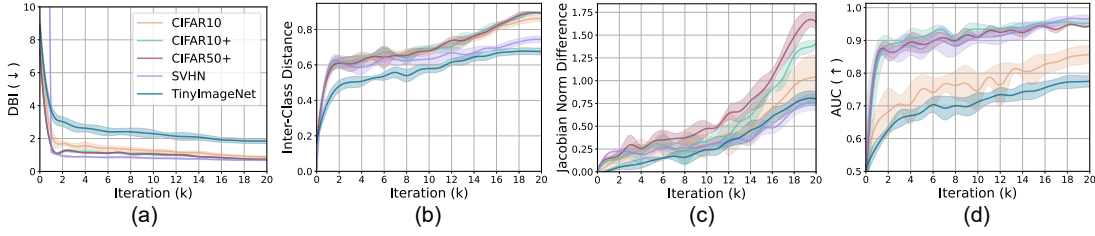


Fig. 4. Several metrics are measured while a discriminative model (ours) is trained. (a) The discriminative quality of known class representations is measured in DBI. (b) The averaged inter-class distances between known classes. (c) The Jacobian norm difference between the known and unknown classes. (d) The degree of separation between known and unknown class representations. **All metrics are improved as the discriminative model learns.**

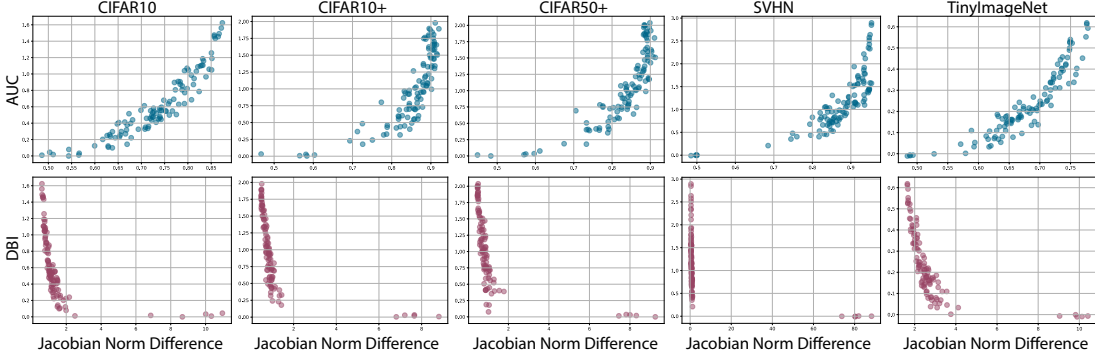


Fig. 5. We measure the detection performance (in AUC), the discriminative quality of known classes (in DBI), and the averaged Jacobian norm difference for a single model during different training iterations, indicating a strong correlation between these metrics.

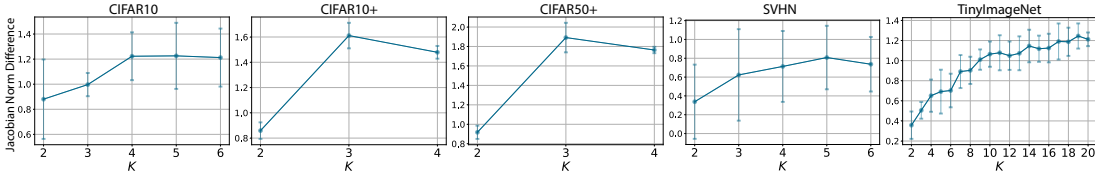


Fig. 6. Increasing the number  $K$  of known classes increases the Jacobian norm difference between the known and unknown classes.

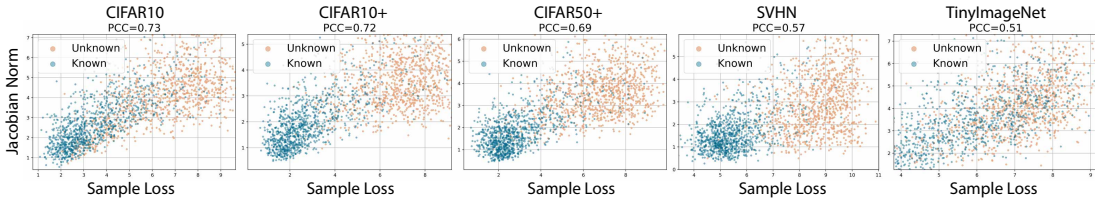


Fig. 7. The correlation between sample-wise losses and the Jacobian norm of the corresponding representations.

class representations. The results are given in Fig. 6 vindicate the consistency of the hypothesis by showing that the Jacobian norm difference becomes larger with a larger number  $K$  of known classes.

## V. METHOD

We develop a method that can effectively improve OSR performance based on our theoretical analysis as a guiding principle. Our method consists of a detection score, a training loss, and subsidiary techniques beneficial for OSR.

### A. Unknown Class Detection by the Model Loss

The analysis in Sec. III indicates that the known and unknown classes are distinguished by their Jacobian norm difference. Hence, one may consider the usage of the Jacobian norm  $S_J(\mathbf{x}) := \left\| \frac{\partial \mathbf{f}}{\partial \mathbf{x}}(\mathbf{x}) \right\|_2$  for unknown class detection score. However, computing the Jacobian norm score  $S_J(\mathbf{x})$  is extremely expensive for high-dimensional data such as images. The Jacobian norm may not capture other factors that separate the unknown class representations. In the latter case, the score function does not detect unknown class samples effectively.

Instead of the Jacobian norm, we may consider the fundamental factor that causes the Jacobian norm difference between

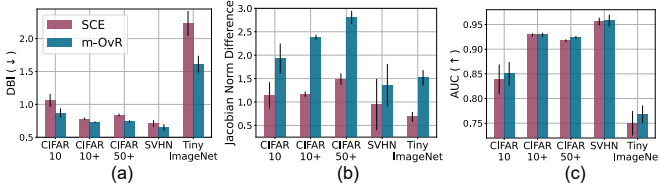


Fig. 8. Comparison of the loss functions (SCE and m-OvR) with respect to (a) the discriminative quality in DBI, (b) Jacobian norm difference, and (c) unknown class detection performance in AUC.

the known and unknown classes, namely, the metric-learning loss function  $\mathcal{L}(\mathbf{x})$ . According to the analysis given in Sec. III, the (minimization of) metric-learning loss function induces the difference between the Jacobian norm of the known class representation and that of the unknown. In this context, our theoretical principle can be comprehensively summarized as

$$\mathcal{L}(\mathbf{x}) \text{ decreases} \\ \implies \mathbb{E}_{\mathbf{x}_u \sim \mathcal{U}} \left[ \left\| \frac{\partial \mathbf{f}}{\partial \mathbf{x}}(\mathbf{x}_u) \right\|_2 \right] - \left\| \frac{\partial \mathbf{f}}{\partial \mathbf{x}}(\mathbf{x}) \right\|_2 \text{ increases} \quad (21)$$

where  $\mathcal{L}(\mathbf{x})$  is a sample-wise metric-learning loss function. Due to Eq. (21), the sample-wise loss will be low over the low Jacobian norm region, and the loss will be high over the high Jacobian norm region. Hence, the metric-learning loss function captures the Jacobian norm difference between the known and unknown.

In addition, the standard metric learning loss quantifies the distance between a query sample and the known classes. Thus, the loss function can capture not only the Jacobian norm separation but also the separation in terms of the distance metric. Motivated upon these observations, we choose the sample-wise loss as the unknown class detection score:

$$S(\mathbf{x}) := \mathcal{L}(\mathbf{x}) := \mathcal{L}(\mathbf{x}, p). \quad (22)$$

Note that the conventional metric loss requires labels  $y$  during its computation. In the inference stage, where no label is provided, we use a pseudo label  $p$  instead.

We empirically observe that the loss function positively correlates to the Jacobian norm, as shown in Fig. 7. In addition, Fig. 7 indicates that the known and unknown are better separated in terms of the sample-wise loss values rather than in the Jacobian norm values. This observation suggests that the loss function captures multiple factors that separate the unknown class representations. Hence, the sample-wise loss is more suitable than the unknown class detection score.

### B. Metric-Learning Loss: marginal One-vs-Rest Loss (m-OvR)

Our analysis indicates that stronger inter-class separation can induce larger Jacobian norm differences and, therefore, better segregation of the unknown class. Thus, for more effective inter-class separation, we adopt representation normalization [26] and one-vs-rest metric learning scheme. Particularly, we unit-normalize the representation vector  $\mathbf{f}(\mathbf{x}) =$

$\hat{\mathbf{f}}(\mathbf{x}) / \|\hat{\mathbf{f}}(\mathbf{x})\|_2$  and similarly the class prototypes. Our training loss function, on the other hand, is given by

$$\mathcal{L}(\mathbf{x}, y) = - \sum_{k=1}^K \mathbb{1}\{y = k\} \log p(k|\mathbf{x}) \\ + \mathbb{1}\{y = k\} \log (1 - p(k|\mathbf{x})) \quad (23)$$

where  $(\mathbf{x}, y)$  is a labeled sample, and  $\mathbb{1}\{\cdot\}$  is an indicator function. The class probability  $p(k|\mathbf{x})$  is given by  $\sigma(Ts_k)$  where  $\sigma$  is the sigmoid activation,  $s_k$  is the similarity between the representation  $\mathbf{f}(\mathbf{x})$  and the  $k$ -th class proxy prototype  $\mathbf{w}_k$ , and  $T$  is a scale term to calibrate the sigmoid probability.

During training, the bare minimization of the loss in Eq. (23) involves a harmful behavior; particularly, minimizing the loss in Eq. (23) collapses the inter-class prototypes as observed by below proposition:

**Proposition 5.** *The minimum OvR loss collapses all prototypes  $\mathbf{w}_k = \mathbf{w}_{k'}$  except  $\mathbf{w}_y$ .*

*Proof.* The proofs of this proposition and the next one are given in Supplementary A.  $\square$

This inter-class collapse misaligns the data representations and corresponding class prototypes. Due to this misalignment, then, the prototype-based similarity  $s_k$  and the model loss function incorrectly capture the class separation in the representation space, thereby degrading the performance of the loss-based unknown class detector.

We mitigate this situation by inserting a margin in the similarity computation; namely, during the training of the OvR metric-learning loss, the similarity is computed by

$$s_k = \cos(\arccos(\mathbf{w}_k \cdot \mathbf{f}(\mathbf{x})) + m) \quad (24)$$

where  $m > 0$  is the margin. The margin ensures an angular gap of degree  $2m$  between inter-class prototypes, thus preventing their collapse:

**Proposition 6.** *For the nonzero margin  $m > 0$ , however, the angle gap can be assured between different prototypes  $\angle(\mathbf{w}_{k_1}, \mathbf{w}_{k_2}) \geq 2m$ .*

We term the OvR loss computed with the margin by marginal-OvR (m-OvR). The effectiveness of margin insertion is verified in the ablation study (Table III). Furthermore, the proposed m-OvR induces strong inter-class separation (below remark) than the standard cross-entropy loss and improves the Jacobian norm difference and unknown class detection performance accordingly.

**Remark (Robust Inter-Class Separation by m-OvR).** Here, we explain why the m-OvR loss induces stronger inter-class separation than the standard softmax cross entropy (SCE) loss. To see this, observe the gradient of SCE loss

$$\frac{\partial \mathcal{L}_{\text{SCE}}}{\partial \theta} = -c \left( \sum_{j \neq y} e^{s_j - s_y} \right) \frac{\partial s_y}{\partial \theta} + c \sum_{k \neq y} e^{s_k - s_y} \frac{\partial s_k}{\partial \theta} \quad (25)$$

where  $\mathcal{L}_{\text{SCE}} = \log(1 + \sum_{k \neq y} e^{s_k - s_y})$  and  $c = (1 + \sum_{j \neq y} e^{s_j - s_y})^{-1}$ . Due to the entanglement of  $s_y$  and  $s_k$  in the exponent, learning can stop (by vanishing gradient) without properly maximizing inter-class separation  $-s_k$ .



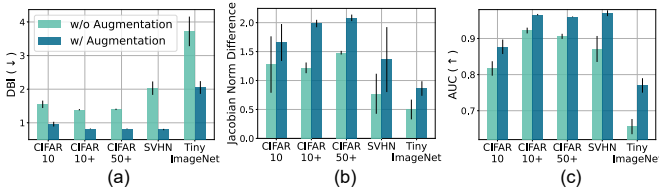


Fig. 9. The effect of data augmentation with respect to (a) the discriminative quality in DBI, (b) Jacobian norm difference, and (c) unknown class detection performance in AUC.

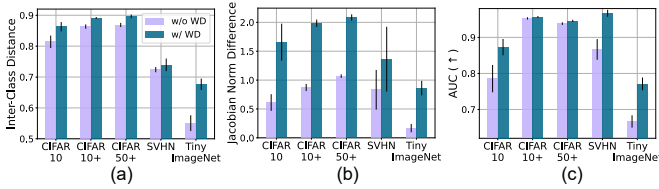


Fig. 10. The effect of weight decay (WD) with respect to (a) averaged inter-class distance, (b) Jacobian norm difference, and (c) unknown class detection performance in AUC.

On the other hand, the inter-class similarity  $s_k$  is (*linearly*) *decoupled* from the intra-class similarity  $s_y$  in the gradient of the m-OvR loss as their corresponding exponents are linearly disentangled. Thus, inter-class distance is maximized independently from the intra-class similarity and hence more effectively. As a result, the m-OvR loss produces better inter-class separation (Fig. 8).  $\square$

The empirical observations given in Fig. 8 indicate the effectiveness of m-OvR compared to the softmax cross entropy (SCE) loss in terms of Jacobian norm difference, discriminative quality of known class representations, and the unknown class detection performance based on the detector in Sec. V-A.

### C. Subsidiary Techniques to Improve OSR

Using the Jacobian norm principle from Sec. III, we explain how the standard techniques (weight decay, auxiliary self-supervision, and data augmentation) improve the separation between known and unknown class representations, thereby improving the OSR performance. Our final model is combined with these techniques.

**Data Augmentation.** The training data is usually limited. Hence, directly applying metric learning to the raw data without augmentation results in suboptimal inter-class separation and intra-class compactness. The Jacobian norm difference between known and unknown class representations would be negligible in this case. Applying data augmentation resolves this issue by expanding the training set size based on the prior human knowledge of the data. Furthermore, the improved Jacobian norm difference by data augmentation enhances the unknown class detection (Fig. 9).

**Weight Decay.** Based on [27], the embedding similarity  $s_k$  is optimized based on the gradient

$$\partial s_k / \partial \hat{\mathbf{f}} = (\mathbf{w}_k - s_k \mathbf{f}) \cdot \|\hat{\mathbf{f}}\|_2^{-1}. \quad (26)$$

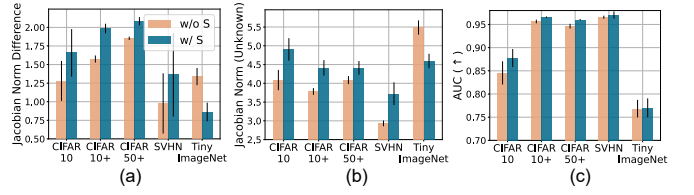


Fig. 11. The effect of auxiliary self-supervision (S) with respect to (a) Jacobian norm difference, (b) Jacobian norm of unknown class, and (c) unknown class detection performance in AUC.

Thus, the small norm  $\|\hat{\mathbf{f}}\|_2$  of the (unnormalized) representation can incite stronger inter-class separation. The weight decay decreases this norm by decreasing the values of the network parameters in  $\hat{\mathbf{f}}$  [28]. Based on our theory, the enhanced inter-class separation results in higher Jacobian norm values of the unknown class representation, resulting in better separation between the known and unknown in the representation space. The experimental results in Fig. 10 precisely verify this theoretical observation.

**Auxiliary Self-Supervision.** To improve the unknown class detection performance, several works [29], [30] employ an auxiliary supervision task to predict the degree of rotation (either 0, 90, 180, or 270) on the rotated images. This extra discriminative task poses additional inter-class separation learning on the model. Based on our observations in Sec. III and IV and Fig. 6, posing additional inter-class separation increases the Jacobian norm of the unknown, thereby improving the separation between the known and unknown class representations (Fig. 11). We note, however, that the auxiliary self-supervision should be accompanied with care; predicting rotation in a standard manner may collapse the original class prototypes  $w_k$  as the rotation prediction head regards the original classes as a single 0-degree class. Hence, we add the auxiliary self-supervision loss  $\mathcal{L}_{self}$  with a small coefficient  $\lambda_{self} = 0.1$ .

Our final metric-learning objective is to minimize the combined loss  $\mathcal{L} + \lambda_{self} \mathcal{L}_{self}$  with data augmentation and weight decay.

## VI. EXPERIMENTS FOR COMPARISON

The experiment section is outlined as follows: (1) We compare our method with other baseline OSR models for the unknown class detection task under two different widely-used protocols, Protocol A [13] and Protocol B [31]. (2) We conduct a careful ablation study of our method, analyzing each component in terms of the unknown class detection performance and the Jacobian norm. (3) We visualize and analyze the Jacobian norm of representation with respect to the metric distances in the representation space. To this end, we compare our proposed model with a baseline model trained with the bare SCE loss.

Our proposed model is trained with the m-OvR loss in all experiments below. Unless specified, we always include weight decay, data augmentation, and auxiliary self-supervision in our model. The default model hyperparameters are as follows: the scale term  $T = 32$ , margin  $m = 0.5$ , the

TABLE I

UNKNOWN CLASS DETECTION PERFORMANCE (IN AUC) AND CLOSED-SET ACCURACY (ACC) FOR OSR WHERE THE UNKNOWN CLASS IS DERIVED FROM THE SAME DISTRIBUTION. THE RESULTS ARE THE AVERAGES FROM 5 RANDOM SPLITS. \* INDICATES THAT THE VALUES ARE TAKEN FROM THE REFERENCES. ‘ARCH.’ DENOTES THE BACKBONE NETWORK USED.

Method	Arch.	CIFAR10		CIFAR10+		CIFAR50+		SVHN		TinyImageNet	
		ACC	AUC	ACC	AUC	ACC	AUC	ACC	AUC	ACC	AUC
<i>Weak Data Augmentation:</i>											
SCE* [13]	VGG	-	67.7	-	81.6	-	80.5	-	88.6	-	57.7
OpenMax* [15]	VGG	80.1	69.5	-	81.7	-	79.6	94.7	89.4	-	57.6
RPL* [17]	VGG	-	82.7	-	84.2	-	83.2	-	93.4	-	68.8
CPN* [19]	VGG	92.9	82.8	-	88.1	-	87.9	96.4	92.7	-	63.9
PROSER* [20]	VGG	92.6	89.1	-	96	-	95.3	96.4	94.3	52.1	69.3
Ours (combined)	VGG	<b>96.4</b>	<b>89.5</b>	<b>96.3</b>	<b>96.2</b>	<b>96.5</b>	<b>95.7</b>	<b>97.4</b>	<b>95.7</b>	<b>78.2</b>	<b>75.3</b>
<i>Weak Data Augmentation:</i>											
SCE	WRN	92.1	76.5	94.0	84.7	94.0	83.8	97.0	92.1	65.8	66.1
N-SCE	WRN	93.7	76.8	93.7	85.3	93.7	84.4	97.1	91.8	64.5	66.4
DOC	WRN	91.6	78.0	93.9	88.2	93.9	88.1	97.0	93.5	59.6	65.5
RPL	WRN	94.7	82.0	95.9	91.1	96.1	90.9	97.5	93.4	71.4	70.4
CPN	WRN	91.2	76.2	93.7	84.6	93.7	83.2	96.7	92.3	59.7	64.6
Ours (combined)	WRN	<b>97.0</b>	<b>89.0</b>	<b>97.7</b>	<b>96.6</b>	<b>97.6</b>	<b>96.0</b>	<b>98.0</b>	<b>97.0</b>	<b>79.1</b>	<b>77.0</b>
<i>Strong Data Augmentation - RandAug (Hyperparameter sensitive):</i>											
SCE* [14]	VGG	-	91.0	-	95.4	-	93.9	-	96.7	-	82.6
<i>Strong Data Augmentation - Flip/Crop/Color Jitter (Standard Hyperparameter):</i>											
SCE	ResNet-18	<b>96.3</b>	91.4	<b>97.4</b>	96.0	<b>97.4</b>	94.2	96.6	97.5	83.1	82.2
m-OvR	ResNet-18	96.0	<b>92.1</b>	97.3	<b>97.7</b>	97.3	<b>95.8</b>	<b>96.8</b>	<b>97.5</b>	<b>83.2</b>	<b>82.9</b>

TABLE II

OSR PERFORMANCE UNDER MACRO-AVERAGED F1-SCORE. \* INDICATES THAT THE VALUES ARE TAKEN FROM THE REFERENCES. ‘ARCH.’ STATES THE BACKBONE NETWORK USED. THE WEIGHT DECAY IS APPLIED IN DEFAULT.

Method	Arch.	Param.	ImageNet-crop	ImageNet-resize	LSUN-crop	LSUN-resize	Avg.
SCE* [31]	VGG	1.1M	63.9	65.3	64.2	64.7	64.5
OpenMax* [31]	VGG	1.1M	66.0	68.4	65.7	66.8	66.7
CROSR* [31]	VGG	1.1M	72.1	73.5	72.0	74.9	73.1
GFROSR* [32]	VGG	1.1M	75.7	79.2	75.1	80.5	77.6
PROSER* [20]	VGG	1.1M	<b>84.9</b>	82.4	<b>86.7</b>	85.6	84.9
Ours	VGG	1.1M	84.2	<b>88.4</b>	85.1	<b>88.1</b>	<b>86.5</b>
SCE	WRN-16-4	2.7M	79.1	79.2	80.3	80.8	79.9
m-OvR	WRN-16-4	2.7M	80.5	79.8	79.2	81.2	80.2
SCE + A	WRN-16-4	2.7M	84.5	88.5	87.0	88.8	87.2
m-OvR + A	WRN-16-4	2.7M	87.4	89.0	89.0	90.0	88.9
SCE + A + S	WRN-16-4	2.7M	84.6	87.5	87.5	87.5	86.8
m-OvR + A + S	WRN-16-4	2.7M	<b>89.1</b>	<b>90.5</b>	<b>90.4</b>	<b>90.9</b>	<b>90.2</b>

auxiliary self-supervision coefficient 0.1, and the weight decay  $1e-3$ .

We consider three backbones to extract the representation: WRN-16-4 [33], VGG [13], and ResNet-18. For WRN-16-4 and VGG, our model is trained by SGD with 20k training iterations unless specified otherwise. Its learning rate is regulated under a cosine scheduler, initiating from 0.1 and decaying to  $1e-5$ . The batch size is 128. In the case of the ResNet-18 backbone, on the other hand, the model is trained for 200 epochs under the SGD optimizer with a momentum of 0.9 and a learning rate of 0.06 that decays to 0 by the cosine learning scheduler.

In all experiments, the model is trained only with known classes so that the model never sees any unknown class sample during training.

#### A. Performance Comparison - Protocol A

**Datasets-Protocol A.** In this protocol [13], we use five different OSR datasets to compare different OSR methods in terms of the closed-set classification accuracy and unknown class detection performance.

Our method is evaluated for unknown class detection performance (AUC) and closed-set accuracy (ACC). The protocol used in [13] is adopted with the following benchmark datasets:

- **CIFAR10 and SVHN:** Among the total ten classes,  $K=6$  classes are chosen as the known ones, regarding the rest as a single unknown class. CIFAR10 [34] consists of generic object images while SVHN [35] of street view numbers.
- **CIFAR10+ and CIFAR50+:** To make CIFAR10 more challenging, CIFAR10+ and CIFAR50+ are considered, in which  $K=4$  known classes are selected from CIFAR10 while 10 (or 50) classes from CIFAR100 [34] constitute a single unknown class.
- **TinyImageNet:** In TinyImageNet (TIN) [36] with more diverse categories,  $K=20$  classes constitutes the known, while the other 180 remaining ones form a single unknown class.

**Results-Protocol A.** The comparison results are given in Table I. We note that we trained our model for 100k iterations for CIFAR10 in the case of weak data augmentation, as it required longer training. Here, weak data augmentation

TABLE III

ABLATION OF OUR PROPOSED MODEL BY ANALYZING ITS TRAINING COMPONENTS: THE M-OvR LOSS, UNIT-NORMALIZATION (N) OF REPRESENTATIONS, THE MARGIN  $m$  IN THE SIMILARITY COMPUTATION, WEIGHT DECAY (W), DATA AUGMENTATION (A), AND AUXILIARY SELF-SUPERVISION (S). MODELS ARE EVALUATED FOR UNKNOWN CLASS DETECTION PERFORMANCE (AUC) IN THE PROTOCOL [13]. SCE SUBSTITUTES IN THE ABSENCE OF M-OvR.

Model	OvR	N	$m$	W	A	S	CIFAR10	CIFAR10+	CIFAR50+	SVHN	TIN	Avg.
Baseline							76.5±2.5	84.7±1.2	83.9±1.2	92.1±1.3	66.1±2.1	80.7±1.7
m-OvR	✓	✓	✓				79.3±2.5	90.1±0.4	89.8±0.4	93.8±1.5	66.2±2.0	83.9±1.4
one out				✓	✓	✓	85.0±1.9	90.4±0.6	89.3±1.0	94.4±1.9	74.7±1.9	86.7±1.5
a		✓		✓	✓	✓	83.9±3.0	92.9±0.3	91.7±0.3	95.6±0.8	75.0 ±2.5	87.8±1.4
b	✓		✓	✓	✓	✓	79.2±3.7	95.7±0.2	94.5±0.3	95.5±1.1	66.1±1.8	86.2±1.4
c	✓	✓	✓	✓	✓	✓	81.7±2.0	92.2±0.8	90.6±0.7	87.1±3.6	65.6±2.1	83.4±1.8
d				✓			81.6±2.6	87.7±0.9	87.1±0.6	94.4±1.2	70.1±2.6	84.3±1.6
e				✓	✓		79.9±2.6	86.8±0.3	85.0±0.5	92.7±1.1	67.3±2.4	82.3±1.4
f	✓	✓	✓	✓			80.3±3.2	89.6±0.4	88.6±0.5	92.8±1.9	68.9±2.3	84.0±1.7
g				✓	✓	✓	84.1±2.6	91.6±0.4	90.8±0.4	95.4±0.5	75.8±2.1	87.5±1.2
h		✓		✓	✓		83.2±3.5	91.1±0.7	90.6±0.6	94.1±1.8	75.6±2.1	86.9±1.7
i	✓	✓	✓	✓	✓		84.6±2.5	95.6±0.4	94.6±0.5	96.6±0.3	76.8±1.9	89.6±1.1
j	✓	✓	✓	✓	✓	✓	85.0±2.4	92.9±0.4	92.4±0.3	95.8±1.2	76.8±1.8	88.6±1.2
k	✓	✓	✓	✓	✓	✓	<b>87.7±2.0</b>	<b>96.6±0.2</b>	<b>96.0±0.1</b>	<b>97.0±0.8</b>	<b>77.0±2.0</b>	<b>90.9±1.0</b>
Ours	✓	✓	✓	✓	✓	✓						

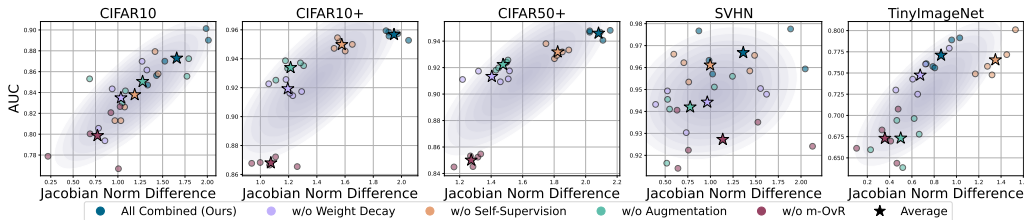


Fig. 12. The plot of Jacobian norm difference versus the unknown class detection performance (AUC). Each point corresponds to a distinct model trained over a different known set, following the protocol of [13]. Different colors indicate different methods. The plot shows the positive correlation, and the all combined model has the largest Jacobian norm difference.

refers to the standard image data augmentation technique that consists of image flipping and translation. In the weak data augmentation, our proposed model outperforms other baselines in both closed-set accuracy and unknown class detection performance, regardless of its embedding backbone architecture. Here, N-SCE indicates the SCE model with unit-normalized representation. Unlike OpenMax and PROSER, Our proposed model does not require post-training [15] nor generated unknown class [20].

Recently, a strong SCE baseline has been found by [14], which shows that the baseline SCE is as effective as the state-of-the-art when accompanied by strong data augmentation, a powerful optimizer, and a carefully selected learning rate scheduler. Inspired by [14], we applied strong data augmentation with our proposed loss. In this case, we do not apply auxiliary self-supervision. To compare fairly, we only vary the loss function from SCE to m-OvR, and everything else remains the same. The strong data augmentation we applied includes color jittering, image crop, and image flip. Note that we did not utilize the RandAug as it was difficult to reproduce, possibly due to the hyperparameter sensitivity of RandAug. The results indicate that the m-OvR loss is more effective than SCE.

*B. Performance Comparison - Protocol B*

**Datasets-Protocol B.** In this experiment, the model is trained over  $K$  known classes and classifies  $K+1$  where the  $K+1$ -th class is the unknown class. The protocol given in [31] is adopted. For benchmarking, we use CIFAR10 classes as the known with  $K=10$ . The unknown class is either ImageNet

[37] or LSUN [38] that comprises scenery images. They are resized or cropped, constituting ImageNet-crop, ImageNet-resize, LSUN-crop, or LSUN-resize. Following the convention given in [20], [31], we choose the threshold  $\tau$  for the inference score in Sec. V-A so that 10% of the validation set is detected as unknown class samples. The performance is evaluated using macro-averaged F1-score [39].

**Results-Protocol B.** The result in Table II shows that our proposed method outperforms all other baselines in the average performance. Under the WRN-16-4 architecture, m-OvR shows superiority over SCE, significantly more effective than SCE when applied with augmentation (A) and self-supervision (S). This is mainly due to the large Jacobian norm difference derived from the highly discriminative representations of the m-OvR (as observed in Fig. 8) triggers a strong separation between the known and unknown class representations.

*C. Ablation Study*

**Ablation on Training Components.** Each component in our model is more carefully evaluated in this experiment. The second block in the row shows that the m-OvR loss outperforms the SCE loss by a large margin, even when there is no data augmentation (A), weight decay (W), and self-supervision (S). The representation embedding normalization (N) improves the performance by preventing trivial increase of the Jacobian norm. The third block in a row (‘one out’) of Table III along with the model-j compares each component by removing one of them out, verifying the effectiveness of each in the entire model. When the standard data augmentation is available (i.e. the fifth block), m-OvR effectively utilizes the data, thus

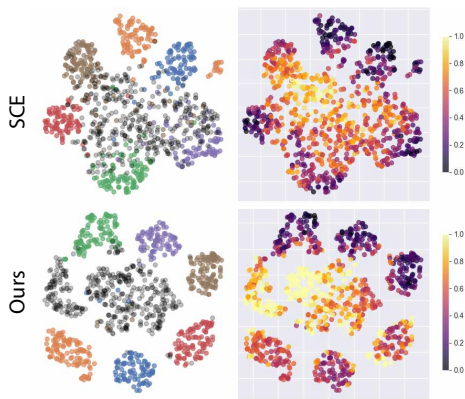


Fig. 13. The 2-dimensional t-SNE [40] visualization of  $f(\mathbf{x})$  trained on MNIST under the protocol of [13]. In the left column, the black color denotes the unknown class. The temperature in the heat map (right column) indicates the (min-max normalized) Jacobian norm  $\|\partial f / \partial \mathbf{x}\|_F$ . The figure shows that the larger the Jacobian norm difference between the known and unknown (i.e., the color contrast in the right column figures), the better the separation between the known and unknown.

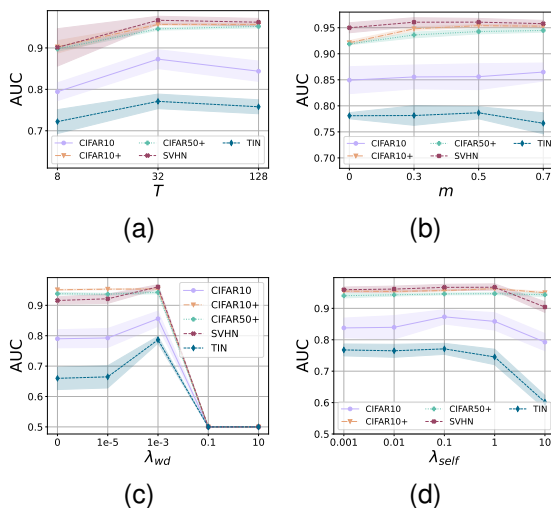


Fig. 14. Unknown class detection performance (AUC) versus (a) the scale  $T$ , (b) the margin  $m$ , (c) the coefficient of the weight decay, and (d) the coefficient of the auxiliary self-supervision loss.

more effectively separating the known from the unknown than SCE. Finally, the sixth block analyzes the margin, which improves the effectiveness of the loss-based unknown class detector by resolving the prototype misalignment issue.

**Ablation with Jacobian Norm Difference** The scatter plot for each fixed dataset in Fig. 12 shows that the degree of separation between the known and unknown class representations positively correlates to the Jacobian norm difference. The correlations in CIFAR10 and TinyImageNet are strong, while CIFAR10+ and CIFAR50+ exhibit some degree of nonlinearity. In SVHN, on the other hand, the correlation is comparatively weak due to the performance saturation. Moreover, this proves that the large Jacobian norm difference is not the only factor that captures distance separation between the known and unknown, as already remarked by Remark III-B2).

**Ablation on Model Hyperparameters.** We analyze the hy-

perparameters of our overall model. Fig. 14 shows that the unknown class detection performance is robust for a sufficiently large scale term  $T$ , and the margin  $m$  should not be too large.

On the other hand, if the weight decay coefficient  $\lambda_{wd}$  is overly large, then it collapses the embedding to a constant (i.e., zero vector). At the same time, overly small  $\lambda_{wd}$  has no impact as a regularizer. Finally, we remark that selecting a proper coefficient for the weight decay is not tricky by observing the train loss dynamic during the early stage.

As already remarked in Sec. V-C, the rotation-based self-supervision auxiliary loss contributes positively only when its coefficient  $\lambda_{self}$  is small (i.e., smaller than 1). The unknown class detection performance is robust for the small values of  $\lambda_{self}$ .

#### D. Visual Analysis of the Jacobian Norm of Representation

In the 2-dimensional visualization of Fig. 13 obtained by applying t-SNE on the embedding representations of data samples, the known classes exhibit small Jacobian norm values while the unknown samples have larger Jacobian norm values. Moreover, the degree of distance-wise separation becomes high when the Jacobian norm contrast between the known and unknown classes is more vivid.

## VII. CONCLUSION

In this work, we exhibited the Jacobian norm of representation embedding as one of the explanatory factors that disclose how closed-set metric learning entails OSR. In particular, the intra/inter-distance optimization lowers the Jacobian norm over the known classes while increasing the norm on the unknown class samples. In turn, the contrast in the Jacobian norm causes the separation of the known from the unknown in the representation space. Taking our theory as a guiding principle, we have developed a method that can effectively improve OSR by combining several techniques that are shown to enhance the Jacobian norm difference.

## REFERENCES

- [1] D. Hendrycks and K. Gimpel, “A baseline for detecting misclassified and out-of-distribution examples in neural networks,” *arXiv preprint arXiv:1610.02136*, 2016.
- [2] K. Lee, K. Lee, H. Lee, and J. Shin, “A simple unified framework for detecting out-of-distribution samples and adversarial attacks,” *Advances in neural information processing systems*, vol. 31, 2018.
- [3] S. Liang, Y. Li, and R. Srikant, “Enhancing the reliability of out-of-distribution image detection in neural networks,” *arXiv preprint arXiv:1706.02690*, 2017.
- [4] C. Geng, S.-j. Huang, and S. Chen, “Recent advances in open set recognition: A survey,” *IEEE transactions on pattern analysis and machine intelligence*, 2020.
- [5] A. Meinke and M. Hein, “Towards neural networks that provably know when they don’t know,” *arXiv preprint arXiv:1909.12180*, 2019.
- [6] A. Meinke, J. Bitterwolf, and M. Hein, “Provably robust detection of out-of-distribution data (almost) for free,” *arXiv preprint arXiv:2106.04260*, 2021.
- [7] S. Liu, R. Garrepalli, T. Dietterich, A. Fern, and D. Hendrycks, “Open category detection with pac guarantees,” in *International Conference on Machine Learning*. PMLR, 2018, pp. 3169–3178.
- [8] Z. Fang, J. Lu, A. Liu, F. Liu, and G. Zhang, “Learning bounds for open-set learning,” in *International Conference on Machine Learning*. PMLR, 2021, pp. 3122–3132.
- [9] L. G. Valiant, “A theory of the learnable,” *Communications of the ACM*, vol. 27, no. 11, pp. 1134–1142, 1984.

- [10] S. Ben-David, J. Blitzer, K. Crammer, F. Pereira *et al.*, “Analysis of representations for domain adaptation,” *Advances in neural information processing systems*, vol. 19, p. 137, 2007.
- [11] A. R. Dhamija, M. Günther, and T. E. Boult, “Reducing network agnostophobia,” *arXiv preprint arXiv:1811.04110*, 2018.
- [12] J. Yang, K. Zhou, Y. Li, and Z. Liu, “Generalized out-of-distribution detection: A survey,” *arXiv preprint arXiv:2110.11334*, 2021.
- [13] L. Neal, M. Olson, X. Fern, W.-K. Wong, and F. Li, “Open set learning with counterfactual images,” in *Proceedings of the European Conference on Computer Vision (ECCV)*, 2018, pp. 613–628.
- [14] S. Vaze, K. Han, A. Vedaldi, and A. Zisserman, “Open-set recognition: A good closed-set classifier is all you need,” *CoRR*, vol. abs/2110.06207, 2021. [Online]. Available: <https://arxiv.org/abs/2110.06207>
- [15] A. Bendale and T. E. Boult, “Towards open set deep networks,” in *Proceedings of the IEEE conference on computer vision and pattern recognition*, 2016, pp. 1563–1572.
- [16] L. Shu, H. Xu, and B. Liu, “Doc: Deep open classification of text documents,” *arXiv preprint arXiv:1709.08716*, 2017.
- [17] G. Chen, L. Qiao, Y. Shi, P. Peng, J. Li, T. Huang, S. Pu, and Y. Tian, “Learning open set network with discriminative reciprocal points,” in *Computer Vision—ECCV 2020: 16th European Conference, Glasgow, UK, August 23–28, 2020, Proceedings, Part III 16*. Springer, 2020, pp. 507–522.
- [18] G. Chen, P. Peng, X. Wang, and Y. Tian, “Adversarial reciprocal points learning for open set recognition,” *arXiv preprint arXiv:2103.00953*, 2021.
- [19] H.-M. Yang, X.-Y. Zhang, F. Yin, Q. Yang, and C.-L. Liu, “Convolutional prototype network for open set recognition,” *IEEE Transactions on Pattern Analysis and Machine Intelligence*, 2020.
- [20] D.-W. Zhou, H.-J. Ye, and D.-C. Zhan, “Learning placeholders for open-set recognition,” in *Proceedings of the IEEE/CVF Conference on Computer Vision and Pattern Recognition*, 2021, pp. 4401–4410.
- [21] H. Zhang, M. Cisse, Y. N. Dauphin, and D. Lopez-Paz, “mixup: Beyond empirical risk minimization,” *arXiv preprint arXiv:1710.09412*, 2017.
- [22] V. Verma, A. Lamb, C. Beckham, A. Najafi, I. Mitliagkas, D. Lopez-Paz, and Y. Bengio, “Manifold mixup: Better representations by interpolating hidden states,” in *International Conference on Machine Learning*. PMLR, 2019, pp. 6438–6447.
- [23] J. Jang and C. O. Kim, “Collective decision of one-vs-rest networks for open-set recognition,” *IEEE Transactions on Neural Networks and Learning Systems*, 2022.
- [24] A. P. Bradley, “The use of the area under the roc curve in the evaluation of machine learning algorithms,” *Pattern recognition*, vol. 30, no. 7, pp. 1145–1159, 1997.
- [25] D. L. Davies and D. W. Bouldin, “A cluster separation measure,” *IEEE transactions on pattern analysis and machine intelligence*, no. 2, pp. 224–227, 1979.
- [26] H. Wang, Y. Wang, Z. Zhou, X. Ji, D. Gong, J. Zhou, Z. Li, and W. Liu, “Cosface: Large margin cosine loss for deep face recognition,” in *Proceedings of the IEEE conference on computer vision and pattern recognition*, 2018, pp. 5265–5274.
- [27] D. Zhang, Y. Li, and Z. Zhang, “Deep metric learning with spherical embedding,” *Advances in Neural Information Processing Systems*, vol. 33, 2020.
- [28] G. Zhang, C. Wang, B. Xu, and R. Grosse, “Three mechanisms of weight decay regularization,” *arXiv preprint arXiv:1810.12281*, 2018.
- [29] D. Hendrycks, M. Mazeika, S. Kadavath, and D. Song, “Using self-supervised learning can improve model robustness and uncertainty,” *arXiv preprint arXiv:1906.12340*, 2019.
- [30] I. Golan and R. El-Yaniv, “Deep anomaly detection using geometric transformations,” *Advances in neural information processing systems*, vol. 31, 2018.
- [31] R. Yoshihashi, W. Shao, R. Kawakami, S. You, M. Iida, and T. Nae-mura, “Classification-reconstruction learning for open-set recognition,” in *Proceedings of the IEEE/CVF Conference on Computer Vision and Pattern Recognition*, 2019, pp. 4016–4025.
- [32] P. Perera, V. I. Morariu, R. Jain, V. Manjunatha, C. Wigington, V. Ordonez, and V. M. Patel, “Generative-discriminative feature representations for open-set recognition,” in *Proceedings of the IEEE/CVF Conference on Computer Vision and Pattern Recognition*, 2020, pp. 11 814–11 823.
- [33] S. Zagoruyko and N. Komodakis, “Wide residual networks,” *arXiv preprint arXiv:1605.07146*, 2016.
- [34] A. Krizhevsky, G. Hinton *et al.*, “Learning multiple layers of features from tiny images,” 2009.
- [35] Y. Netzer, T. Wang, A. Coates, A. Bissacco, B. Wu, and A. Y. Ng, “Reading digits in natural images with unsupervised feature learning,” 2011.
- [36] Y. Le and X. Yang, “Tiny imagenet visual recognition challenge,” *CS 231N*, vol. 7, no. 7, p. 3, 2015.
- [37] O. Russakovsky, J. Deng, H. Su, J. Krause, S. Satheesh, S. Ma, Z. Huang, A. Karpathy, A. Khosla, M. Bernstein *et al.*, “Imagenet large scale visual recognition challenge,” *International journal of computer vision*, vol. 115, no. 3, pp. 211–252, 2015.
- [38] F. Yu, A. Seff, Y. Zhang, S. Song, T. Funkhouser, and J. Xiao, “Lsun: Construction of a large-scale image dataset using deep learning with humans in the loop,” *arXiv preprint arXiv:1506.03365*, 2015.
- [39] Y. Sasaki, “The truth of the f-measure,” *Teach Tutor Mater*, 01 2007.
- [40] L. Van Der Maaten, “Learning a parametric embedding by preserving local structure,” in *Artificial Intelligence and Statistics*. PMLR, 2009, pp. 384–391.

# Supplementary

## APPENDIX

### A. Jacobian Norm Analysis of the Softmax Cross Entropy Model

The results given in 15 show that the Jacobian norm trend that we observed in the main sections holds the same way for the softmax cross entropy models.

### B. Other Proofs

**Propositions 5 and 6.** With the optimal prototypes  $\{\mathbf{w}_k\}_{k=1}^K$  for a single sample representation  $\mathbf{f}(\mathbf{x})$  paired with label  $y$ , we have the collapse  $\mathbf{w}_k = -\mathbf{w}_y$  for all  $k \neq y$  if  $m_n = 0$ , while  $\angle(\mathbf{w}_k, -\mathbf{w}_y) \geq m_n$  with  $k \neq y$  if  $0 < m_n < \pi/2$ .

*Proof of Propositions 5 and 6.* For the optimal prototypes  $\{\mathbf{w}_k\}_{k=1}^K$ , we have  $s_y = \max_{\mathbf{w}_y} s_y$  and  $s_k = -1$ . Regardless of whether  $m_n > 0$  or not, we have  $\mathbf{f}(\mathbf{x}) = \mathbf{w}_y$ . For the negative pair, if  $m_n = 0$ , then  $\mathbf{f}(\mathbf{x}) = \mathbf{w}_k$ , and hence  $-\mathbf{w}_y = \mathbf{w}_k$  for all  $k \neq y$ . If  $m_n > 0$ , then  $s_k = -1$  when the angle between  $\mathbf{w}_k$  and  $\mathbf{f}(\mathbf{x})$  is  $\pi - m_n$ , implying that  $\angle(\mathbf{w}_k, -\mathbf{w}_y) = \angle(\mathbf{w}_k, -\mathbf{f}(\mathbf{x})) = m_n$ , finishing the proof.  $\square$

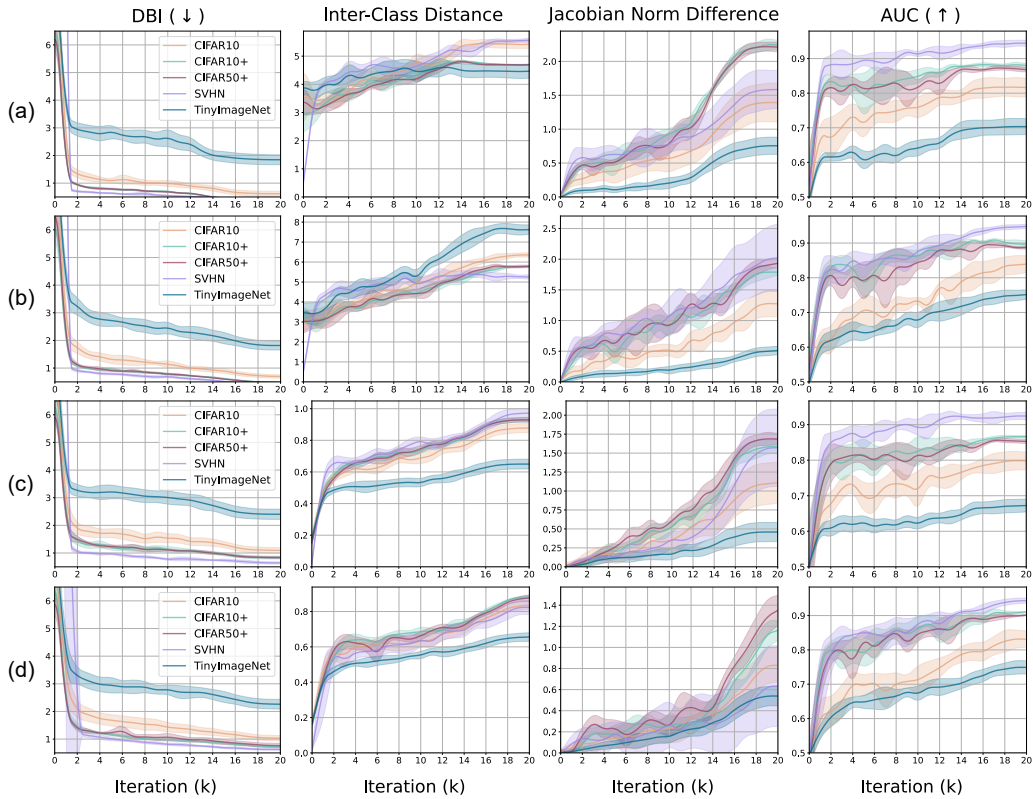


Fig. 15. Several metrics measured while different discriminative models are begin trained. (a) SCE without data augmentation, (b) SCE with data augmentation, (c) SCE with normalized embedding but without data augmentation, (d) SCE with normalized embedding and data augmentation.